

THE *CHANDRA* VIEW OF THE SUPERNOVA REMNANT 0506–68.0 IN THE LARGE MAGELLANIC CLOUDJOHN P. HUGHES¹, MARC RAFELSKI², JESSICA S. WARREN¹, CARA RAKOWSKI³, PATRICK SLANE³, DAVID BURROWS⁴, AND JOHN NOUSEK⁴*Received 2006 April 5; accepted 2006 May 31*

ABSTRACT

A new *Chandra* observation of SNR 0506–68.0 (also called N23) reveals a complex, highly structured morphology in the low energy X-ray band and an isolated compact central object in the high energy band. Spectral analysis indicates that the X-ray emission overall is dominated by thermal gas whose composition is consistent with swept-up ambient material. There is a strong gradient in ambient density across the diameter of the remnant. Toward the southeast, near a prominent star cluster, the emitting density is 10^{-23} cm^{-3} , while toward the northwest it has dropped to a value of only 1 cm^{-3} . The total extent of the X-ray remnant is $100'' \times 120''$ (24 pc \times 29 pc for a distance of 50 kpc), somewhat larger than previously known. The remnant's age is estimated to be ~ 4600 yr. One part of the remnant shows evidence for enhanced O, Ne, and perhaps Mg abundances, which is interpreted as evidence for ejecta from a massive star core collapse supernova. The compact central object has a luminosity of a few times $10^{33} \text{ ergs s}^{-1}$ and no obvious radio or optical counterpart. It does not show an extended nebula or pulsed emission as expected from a young energetic pulsar, but resembles the compact central objects seen in other core collapse SNe, such as Cas A.

Subject headings: ISM: individual (LHA 120-N 23, SNR 0506–68.0) — shock waves — supernova remnants — X-rays: individual (CXOU J050552.3–680141) — X-rays: ISM

1. INTRODUCTION

The *Chandra X-ray Observatory* has been a revolutionary tool for studying supernova remnants (SNRs) in the Large Magellanic Cloud (LMC). The telescope's superb spatial resolution has revealed newly processed metals in the interiors of most LMC SNRs and at least one new pulsar wind nebula (see Weisskopf & Hughes 2005, and reference therein). Studying the full sample of LMC SNRs is essential to gain a more complete understanding of the evolution of metal-rich ejecta from its synthesis in stars and SNe to its integration into the interstellar medium.

Although relatively bright in the radio and X-ray bands (it is ranked ninth brightest in the soft X-ray band and eleventh brightest at 408 MHz; Mathewson et al. 1983), SNR 0506–68.0 (also called N23) has not been extensively studied. Chu & Kennicutt (1988) suggest that it had a massive star progenitor due to the high density of OB stars in the environment and its close proximity to H II regions and star clusters. There is a strong gradient in brightness across the remnant in the X-ray (Mathewson et al. 1983) and radio (Dickel & Milne 1998) bands. Its integrated X-ray emission (Hughes et al. 1998) is dominated by soft thermal emission from swept-up ambient medium with the lowered abundances (~ 0.3 solar) typical of the LMC.

According to Mathewson et al. (1983), SNR 0506–68.0 is an intermediate sized remnant (~ 11 pc in diameter). All smaller LMC remnants show evidence for youth (i.e.,

an energetic pulsar or ejecta-dominated emission), while nearly all larger remnants are dominated by swept-up ambient medium (Hughes et al. 1998). Of course, size alone is an imperfect predictor of evolutionary state, yet the possibility that SNR 0506–68.0 is in a transitional stage of evolution (between ejecta-dominated and Sedov) makes it worth studying. The original goals of our observation were to find and categorize X-ray-emitting SN ejecta, search for a pulsar-powered synchrotron nebula or other compact X-ray star, and clarify the evolutionary state of SNR 0506–68.0 through spatially resolved X-ray spectroscopy to better understand the nature of its progenitor star and its effects on the local environment. While this work was being completed, an independent report (Hayato et al. 2006a,b) noting a spectrally hard, X-ray compact object in N23 came to our attention. In the following we present the results of our comprehensive exposition of the *Chandra* data in which we arrive at a different conclusion regarding the nature of the compact star. Throughout, we assume a distance of 50 kpc to the LMC.

2. DATA REDUCTION AND ANALYSIS

We observed SNR 0506–68.0 with *Chandra* on 2002 Dec 29 using the ACIS-S detector in full-frame timed exposure mode (ObsId 2762). Standard cleaning procedures were applied to the data including filtering for times of high background that resulted in a useful live-time corrected exposure of 34744 s. Event pulse heights were corrected for time dependent gain effects and spectral response func-

¹ Department of Physics and Astronomy, Rutgers University, 136 Frelinghuysen Road, Piscataway, NJ 08854-8019; jph@physics.rutgers.edu, jesawyer@physics.rutgers.edu

² UCLA, Physics and Astronomy Building, 430 Portola Plaza, Box 951547, Los Angeles, CA 90095-1547; marcar@astro.ucla.edu

³ Harvard-Smithsonian Center for Astrophysics, 60 Garden Street, Cambridge, MA 02138; rakowski@head-cfa.harvard.edu, slane@head-cfa.harvard.edu

⁴ Department of Astronomy and Astrophysics, Pennsylvania State University, 525 Davey Laboratory, University Park, PA. 16802; dxb15@psu.edu, nousek@astro.psu.edu

tions accounted for absorption due to contamination build-up on the ACIS filters. The optical field of the SNR is quite crowded and it was not possible to identify unambiguous counterparts to serendipitous *Chandra* sources and thereby improve the astrometric accuracy of the X-ray data. Nevertheless the observation is not affected by any known aspect offset and therefore we expect the absolute positional uncertainty to be 0.6" (radius, at 90% confidence).

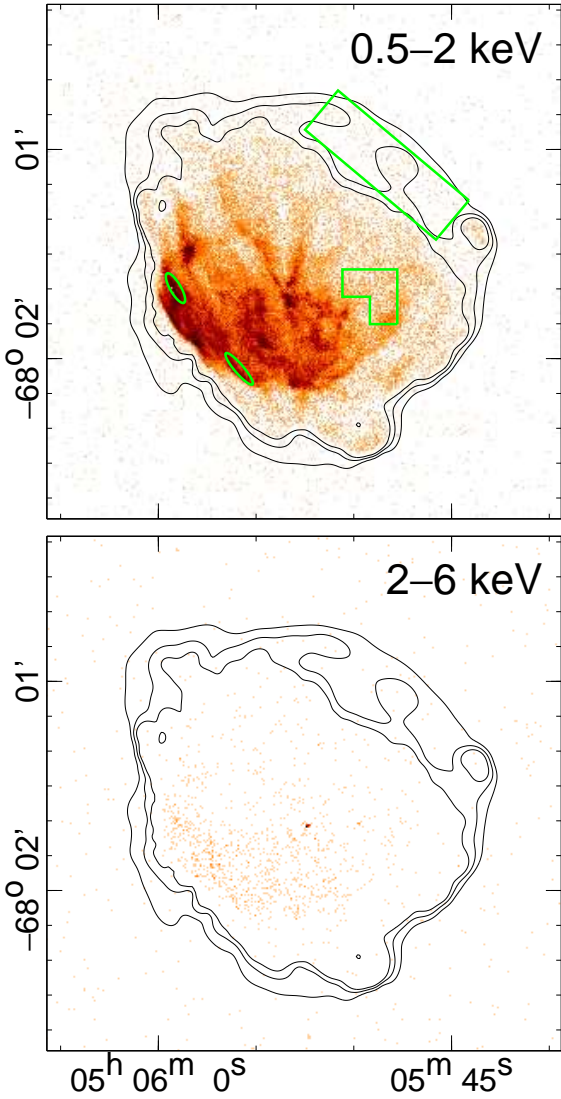


FIG. 1.— Soft (top) and hard (bottom) band *Chandra* X-ray images of SNR 0506–68.0. Spectral extraction regions are shown in green in the top panel. Contours delineate the faintest outer extent of the remnant from a smoothed image.

2.1. Gaseous Remnant

Figure 1 shows *Chandra* images of SNR 0506–68.0 in two broad energy bands (0.5–2 keV and 2–6 keV) along with contours indicating the faint outermost extent of the remnant from an adaptively smoothed image (not shown). Nearly all of the X-ray emission occurs below 2 keV except for a central compact object (see below) and some of the brightest portions of the limb. Those bright portions lie mostly toward the east and southeast and appear highly structured and filamentary. The northwestern half of the remnant is much fainter and shows a hint of

limb-brightening. The overall extent of the remnant is 100" × 120", larger than previous estimates of the X-ray size (Mathewson et al. 1983; Williams et al. 1999). The integrated X-ray spectrum (Fig. 2) clearly indicates the characteristics of soft thermal emission and closely resembles the *ASCA* spectrum (Hughes et al. 1998).

TABLE 1
SPECTRAL MODEL FIT RESULTS FOR SNR FILAMENTS

Parameter	Value and Uncertainty (1 σ)	
	East rim	Southeast rim
$N_{\text{H}}(\text{LMC})$ (H atoms cm^{-2})	$3.3_{-0.07}^{+0.10} \times 10^{21}$	$2.1_{-0.1}^{+0.4} \times 10^{21}$
kT (keV)	0.48 ± 0.14	0.77 ± 0.4
$\log_{10}(n_{\text{e}}t/\text{cm}^{-3}\text{s})$	$10.6_{-0.3}^{+0.5}$	11.2 ± 0.3
Oxygen	0.15 ± 0.05	0.30 ± 0.18
Neon	0.23 ± 0.09	0.32 ± 0.09
Magnesium	0.18 ± 0.13	0.21 ± 0.17
Iron	0.13 ± 0.06	0.20 ± 0.15
$n_{\text{e}}n_{\text{H}}V/(4\pi D^2)$ (cm^{-5})	9.75×10^{10}	2.28×10^{10}
$\chi^2/\text{d.o.f}$	94.8/56	42.4/49

Two representative spectra from portions of the bright eastern rim (hereafter east rim and southeast rim, indicated by the two ellipses on Fig. 1) were extracted, regrouped to contain at least 20 counts per channel, and analyzed with planar-shock nonequilibrium ionization (NEI) models (Hughes et al. 2000). The fits included Galactic absorption with solar composition and column density fixed to the value 5.8×10^{20} atoms cm^{-2} from Dickey & Lockman (1990) and LMC absorption with variable $N_{\text{H}}(\text{LMC})$ and metal abundances of 0.3 times solar. Numerical results are given in Table 2.1 and the spectral data with best-fitted models are plotted in Fig. 2 (as blue and green curves). Only the abundances of O, Ne, Mg, and Fe in the emission model were allowed to vary freely, all other species had their abundances fixed to 0.3 times solar. The derived abundances clearly show that the bright rim emission is dominated by gas with LMC composition. We also extracted the spectrum of the faint western limb as well (from the large rectangular region to the west of Fig. 1). All elemental abundances were fixed to 0.3 times solar, because of the low statistics of this spectrum (~ 220 counts above background). Furthermore the uncertainties on the fitted thermodynamic quantities are large, so we only quote best fit values as indicators of the thermodynamic state: $N_{\text{H}}(\text{LMC}) \sim 7 \times 10^{21}$ H atoms cm^{-2} , $kT \sim 0.3$ keV, $\log_{10}(n_{\text{e}}t/\text{cm}^{-3}\text{s}) \sim 9.8$, and $n_{\text{e}}n_{\text{H}}V/(4\pi D^2) \sim 4.5 \times 10^{10}$ cm^{-5} . The fit was statistically acceptable ($\chi^2 = 7.2$ for 8 degrees of freedom).

Numerous spectra were extracted from elsewhere across the remnant including both filament and inter-filament regions, but in nearly all cases the gas composition was consistent with LMC abundances. Only one region showed any evidence for elevated abundances (the inverted "L"-shaped region in Fig. 1). This spectrum's relatively strong emission around 0.6 keV (see cyan curve in Fig. 2) clearly sets it apart from the rim spectra discussed above. Our spectral fit prefers high temperatures (> 0.7 keV) and enhanced abundances for O (> 0.7) and Ne (> 0.8), and perhaps Mg (> 0.3). Note that these values represent the 90% confidence lower bound on the parameters. Over this

range the Fe abundance is clearly constrained to be at or below the LMC value. For temperatures lower than 0.7 keV, the abundance ratio of O to Fe (relative to solar) grows even larger and at 0.5 keV the ratio is >20 . Although the precise values are somewhat indeterminant, we conclude with some confidence that the low Z elements are enhanced in this particular part of the remnant.

2.2. Compact Star

Close to the geometric center of the SNR an isolated X-ray point source (hereafter CXOU J050552.3–680141) is clearly seen in the 2–6 keV band (Fig. 1) at a position of RA=05:05:52.32, Decl.=−68:01:41.2 (epoch J2000). The detection in this hard X-ray band is significant; we obtain 31 net counts within a 2 pixel radius with an expectation value from background alone of 1.4 counts. The source is also detected in the soft band (0.5–2 keV) at approximately the same significance level. The net (local background subtracted) count rate of the source in the 0.5–6 keV band is $(2.8 \pm 0.4) \times 10^{-3} \text{ s}^{-1}$.

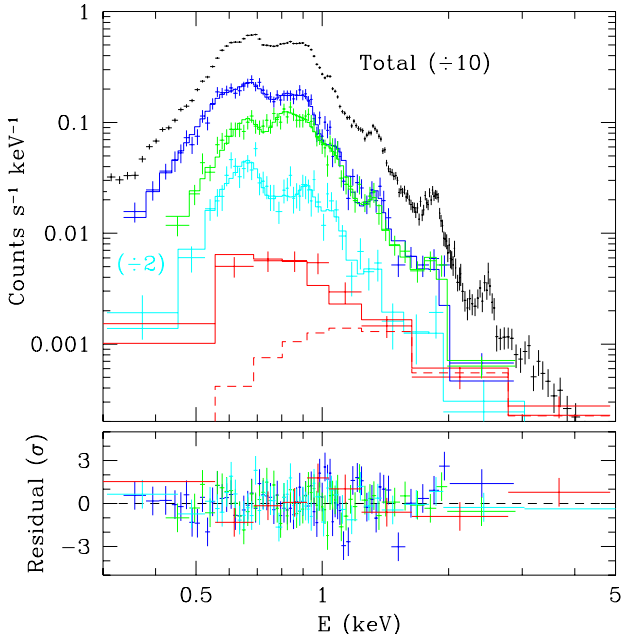


FIG. 2.— Spectra and best fit models for several positions in SNR 0506–68.0. In order from the top the spectra are from the entire remnant (black), the east bright rim (blue), southeast rim (green), enhanced abundance region (cyan), and the central compact object (red).

We simulated the *Chandra* point-spread-function (PSF) at the observed position of the compact object using *Chandra* Ray Tracer (ChaRT).⁵ The observed structure and radial profile of the star are entirely consistent with the PSF and we find no evidence for extended emission (for a close-up view of the point source see the insert box in Fig. 3).

⁵ ChaRT is available on-line at: <http://asc.harvard.edu/chart/index.html>

TABLE 2
SPECTRAL MODEL FIT RESULTS FOR COMPACT SOURCE

Parameter	Value and Uncertainty (1 σ)
Power Law Model	
$N_{\text{H}}(\text{LMC})$ (H atoms cm^{-2})	$3.7_{-2.4}^{+2.0} \times 10^{21}$
α_{P}	$1.5_{-0.6}^{+0.7}$
$F_{\text{Fe}}(1 \text{ keV})$ (photon $\text{s}^{-1} \text{ cm}^{-2} \text{ keV}^{-1}$)	$4.5_{-2.1}^{+2.9} \times 10^{-6}$
$\chi^2/\text{d.o.f}$	10.0/5
Blackbody Model	
$N_{\text{H}}(\text{LMC})$ (H atoms cm^{-2})	$5.7_{-1.4}^{+1.5} \times 10^{21}$
kT (keV)	$0.96_{-0.20}^{+0.36}$
Norm $(R/1 \text{ km})^2/(D/10 \text{ kpc})^2$	$3.5_{-2.6}^{+1.6} \times 10^{-3}$
$\chi^2/\text{d.o.f}$	12.9/5

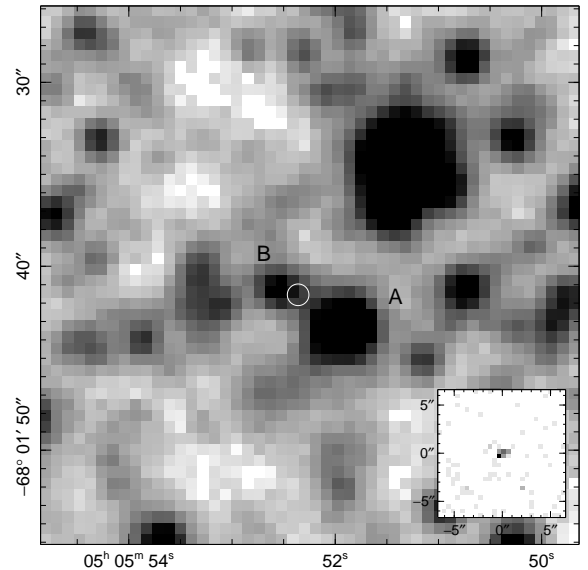


FIG. 3.— Broad band blue optical image from the MACHO project in the vicinity of the compact central X-ray source. Stars labeled A and B are closest to the X-ray source, whose error circle is shown in white. The X-ray data in the 2–6 keV band are shown in the small insert figure to the lower right. The slight E–W extent of the X-ray source is entirely due to the *Chandra* PSF at this location.

The spectrum of the compact source was extracted from a circular region 2 pixels (0.984'') in radius. The main source of background comes from thermal emission emitted by the gaseous remnant itself, which accounts for half the extracted counts (~ 100 out of 193 total). Our spectral fit for the compact star, therefore, included a NEI thermal component with variable intensity, but fixed abundance (0.3 times solar), temperature and ionization timescale. The latter two quantities were determined by a spectral fit to data extracted from an annulus surrounding the point source covering 4–6 pixels in radius. Emission from the compact star was assumed to be either a blackbody or a power-law. Absorption, including Galactic and LMC components, was included as above. Table 2.2 shows the

results and the spectral data and model are plotted in Fig. 2 (in red). The red dashed curve shows the best fit power-law model for the compact star's emission. The luminosity of the compact source under the power law spectral model is $L_X \sim 2 - 5 \times 10^{33} \text{ erg s}^{-1}$ (0.5–2 keV) and $L_X \sim 3 - 6 \times 10^{33} \text{ erg s}^{-1}$ (2–6 keV). The blackbody fits yield similar values: $L_X \sim 0.8 - 2 \times 10^{33} \text{ erg s}^{-1}$ (0.5–2 keV) and $L_X \sim 3 - 6 \times 10^{33} \text{ erg s}^{-1}$ (2–6 keV).

Using FFT and epoch folding techniques we searched for a pulsed signal from the compact object. Nothing significant was found for frequencies of several mHz up to the Nyquist limit (~ 0.154 Hz), which was set by the intrinsic time resolution (~ 3.24 s) of our ACIS observation mode. We are unable to set interesting limits on the pulsed fraction because of the faintness of the source in comparison to the contaminating remnant flux even within a $\sim 1''$ radius extraction region.

Radio images (Dickel & Milne 1998) from the ATCA show no evidence for the compact source in any of the four wavelengths mapped (3.5 cm, 6 cm, 13 cm, and 20 cm) to an estimated flux limit of ~ 2 mJy. These limits are a factor of ~ 20 below the radio flux of the pulsar wind nebula in SNR 0453–685 (Gaensler et al. 2003), whereas the X-ray source in SNR 0506–68.0 is only a factor of two fainter than the source in SNR 0453–685. Clearly CXOU J050552.3–680141 is relatively radio quiet. There is also no clear optical counterpart in the DSS, but the field is crowded and the flux limit is high. We obtained public domain images from the MACHO Project that allowed us to set a more sensitive limit. In Fig. 3 we show a portion of an image made by stacking 10 individual 300-s exposures with moderately good seeing. The combined image was registered to the sky using several hundred HST guide stars for a positional accuracy of $< 0.3''$ in each axis. A subset of these stars was also used to estimate a coarse photometric zero point for the image (accurate to roughly ± 0.3 mag). The nearest stars are $3.4''$ (star A) and $1.1''$ (star B) away from the X-ray compact object and are therefore nominally outside the *Chandra* error circle as indicated by the circle in the figure. The estimated magnitudes of these stars are ~ 17 (A) and ~ 19 (B).

3. CONCLUSIONS AND SUMMARY

There is a strong gradient in density from east to west across SNR 0506–68.0 as hinted at by the brightness gradient. The emitting gas density can be determined from the fitted emission measure and a simple geometric estimate for the volume. The east rim spectrum comes from a region $\sim 10''$ long by $\sim 3''$ thick. Assuming the depth in the line-of-sight is the same as its length, we find a volume of $6.4 \times 10^{55} \text{ cm}^3$, which results in a hydrogen number density of 23 cm^{-3} . The southeast rim spectrum yields a similar density estimate of 10 cm^{-3} . We estimate the emission volume of the west rim spectrum (extracted from a region of size $50'' \times 15''$) to be $\sim 1.5 \times 10^{58} \text{ cm}^3$ which leads to a density estimate of 1 cm^{-3} . There is more than a factor of 10 variation in the ambient medium density from east to west. We can estimate “shock” ages from the densities just derived and the ionization timescales in Table 2.1. We

find values of 55 yrs for the east rim and 500 yrs for the southeast rim, albeit with large errors. This suggests that the SN shock wave has encountered some portions of the bright eastern limb more recently than others. To conclude this discussion of the remnant's environment we note that the open cluster HS114 (Hodge & Sexton 1966) lies on the high density side of the remnant; the bright X-ray limb (near the east rim region) is only some $8''$ (2 pc) from the edge of the cluster.

The complex morphology of SNR 0506–68.0 revealed by our new *Chandra* data makes it clear that estimates of its dynamical state based on global properties (e.g., size, brightness, integrated spectrum) are questionable. We make the unjustified but plausible assumption that the remnant's evolution toward the low density northwest hemisphere can be described by an adiabatic Sedov-phase model. The radius of the remnant in this direction is $\sim 50''$ (12 pc) and the ambient density, using the results in the previous paragraph, is $\sim 0.25 \text{ cm}^{-3}$. With these values and a canonical explosion energy of 10^{51} ergs the age of SNR 0506–68.0 is ~ 4600 yrs.

The high density environment, proximity to a young star cluster, and presence of enhanced low-Z metal abundances in the remnant all point toward a core collapse SN and massive star progenitor for SNR 0506–68.0. A neutron star (or, more speculatively, a black hole) is therefore a plausible identification for the compact central X-ray star. The lack of an extended nebula and the relatively low radio-to-X-ray flux ratio argue against a young, rapidly-rotating, high spin-down-rate pulsar. However the X-ray luminosity (a few times $10^{33} \text{ erg s}^{-1}$) and spectrum (e.g., $kT_{\text{BB}} \sim 0.75 - 1.3$ keV) are broadly consistent with the emerging class of central compact X-ray-emitting objects such as the one in Cas A (Pavlov et al. 2000) that are believed to be isolated neutron stars. Unfortunately the current optical magnitude limits cannot definitively rule out an extragalactic origin for the X-ray source, although the star's location very near the center of SNR 0506–68.0 gives strong support for a physical association. An unambiguous identification of the X-ray source will require further study across the electromagnetic spectrum.

This paper utilizes public domain data originally obtained by the MACHO Project, whose work was performed under the joint auspices of the U.S. Department of Energy, National Nuclear Security Administration by the University of California, Lawrence Livermore National Laboratory under contract No. W-7405-Eng-48, the National Science Foundation through the Center for Particle Astrophysics of the University of California under cooperative agreement AST-8809616, and the Mount Stromlo and Siding Spring Observatory, part of the Australian National University. We also acknowledge J. Dickel and P. Ghavamian, who helped with various aspects of this research. Partial support was provided by *Chandra* grant no. GO2-3069X to Rutgers University, NASA grant no. NAG5-9281 to SAO, and NASA Contract NAS8-39073 to SAO.

REFERENCES

Chu, Y.-H., & Kennicutt, R. C., Jr. 1988, AJ, 96, 1874
 Dickel, J. R., & Milne, D. K. 1998, AJ, 115, 1057
 Dickey, J. M., & Lockman, F. J. 1990, ARA&A, 28, 215
 Gaensler, B. M., Hendrick, S. P., Reynolds, S. P., & Borkowski, K. J. 2003, ApJ, 594, L111
 Hodge, P. W., & Sexton, J. A. 1966, AJ, 71, 363
 Hayato, A., Bamba, A., & Tamagawa, T. 2006, abstract submitted for July COSPAR meeting, Beijing
 Hayato, A., Bamba, A., Tamagawa, T., & Kawabata, K. 2006, ApJ, submitted
 Hughes, J. P., Hayashi, I., Koyama, K. 1998, ApJ, 505, 732
 Hughes, J. P., Rakowski, C. E., & Decourchelle, A. 2000, ApJ (Letters), 543, L61
 Mathewson, D. S., Ford, V. L., Dopita, M. A., Tuohy, I. R., Long, K. S., & Helfand, D. J. 1983, ApJS, 51, 345
 Pavlov, G. G., Zavlin, V. E., Aschenbach, B., Trümper, J., & Sanwal, D. 2000, ApJ, 531, L53
 Weisskopf, M. C., & Hughes J. P. 2005, Astrophysics Update 2, ed. J. W. Mason, (Springer: Berlin), 55
 Williams, R. M., Chu, Y.-H., Dickel, J. R., Petre, R., Smith, R. C., & Tavarez, M. 1999, ApJS, 123, 467